Research Square

Preprints are preliminary reports that have not undergone peer review.
They should not be considered conclusive, used to inform clinical practice,
or referenced by the media as validated information.

Geophysical evidence of structural and topographic controls on the Tulancingo Valley aquifer system, Central Mexico

Diego A. Aguilar-Anaya

diegoaaa@igeofisica.unam.mx

Universidad Nacional Autónoma de México

Gonzalo Cid-Villegas

Centro de Estudios Superiores Isla del Carmen

Francisco Chacón-Hernández

Universidad Nacional Autónoma de México

Abner I. Sánchez-Andrade

Geotem Ingeniería

Research Article

Keywords: Tulancingo Valley aquifer, overexploitation, resistivity, electromagnetics, static water level

Posted Date: November 10th, 2026

DOI: https://doi.org/10.21203/rs.3.rs-11374961/v1

License: This work is licensed under a Creative Commons Attribution 4.0 International License.
Read Full License

Additional Declarations: No competing interests reported.

Geophysical evidence of structural and topographic controls on the Tulancingo Valley aquifer system, Central Mexico

Diego A. Aguilar-Anaya [a*], Gonzalo Cid-Villegas [b], Francisco Chacón-Hernández [c], Abner I. Sánchez-Andrade [d]

[a] Facultad de Ingeniería, Universidad Nacional Autónoma de México, Mexico City, Mexico.
https://orcid.org/0009-0004-6864-9444

[b] Centro de Estudios Superiores Isla del Carmen, Campeche, Mexico.
https://orcid.org/0009-0001-7250-4705

[c] Instituto de Geofísica, Universidad Nacional Autónoma de México, Mexico City, Mexico.
https://orcid.org/0000-0002-9664-2272

[d] Geotem Ingeniería, Mexico City, Mexico.
https://orcid.org/0009-0003-0826-6057

Corresponding author: Diego A. Aguilar-Anaya: diegoaaa@igeofisica.unam.mx; diegore013@gmail.com and Francisco Chacón-Hernández: chaconf@igeofisica.unam.mx

Abstract

The Tulancingo Valley aquifer, located in southeastern Hidalgo state, central-eastern Mexico, is one of the most overexploited groundwater resources. To characterize its hydrogeological framework and the mechanisms driving deviations in the static water level, an integration of gravimetric data, transient electromagnetic (TEM) soundings and electrical resistivity tomography (ERT) was implemented. Residual gravity data delineate prominent NW-SE and NE-SW structural lineaments associated with the Acoculco caldera

and regional normal faulting, while resistivity models identify two hydraulically connected systems separated by a faulted volcanic aquitard: a shallow aquifer (up to 20 m depth; ~2–15 Ω·m) and a heavily exploited deep regional aquifer (reaching depths of 130–250 m; ~2–20 Ω·m). The regional structural features exert a primary control on the hydrodynamics of the deep aquifer. These fault and fracture networks lead to hydraulic connectivity and partitioned groundwater flow, directly influencing the spatial distribution of static water level variations. Projections indicate that under this structurally controlled flow regime, current extraction trends will drive water deficits to 23.64 Mm^3 and 31.64 Mm^3 by 2030 and 2050, respectively. These findings provide a geophysical base for sustainable groundwater management in structurally complex aquifer systems.

Keywords: Tulancingo Valley aquifer, overexploitation, resistivity, electromagnetics, static water level.

1. Introduction

Groundwater stored in aquifers is a critical resource for socioeconomic development, supporting agriculture, public consumption, industry, and energy production. However, aquifer systems worldwide are increasingly threatened by contamination and overexploitation. Overexploitation occurs when extraction exceeds average annual recharge, while groundwater pollution often results from inadequate agricultural, industrial, or domestic practices (1). These pressures compromise both the availability and sustainability of groundwater, particularly in regions with intensive water use.

In Mexico, the National Water Commission (CONAGUA) has classified several aquifers as overexploited (https://sigagis.conagua.gob.mx/dma230911/). Within the state of Hidalgo, which contains 21 aquifers, the Tulancingo Valley aquifer is the most stressed system (Fig. 1). By 2023, over 300 concessions had been granted, and the proliferation of new groundwater wells (green circles in Fig. 1) has significantly intensified pressure on the system. Consequently, the aquifer's volume deficit has more than doubled over the last two decades, rising from 9.78 Mm^3 in 2006 to 22.6 Mm^3 in 2024 (2). Beyond depletion, water quality deterioration has been documented, with contaminants from dairy industry activities detected in springs and wells throughout the valley (3, 4, 5, 6, 7).

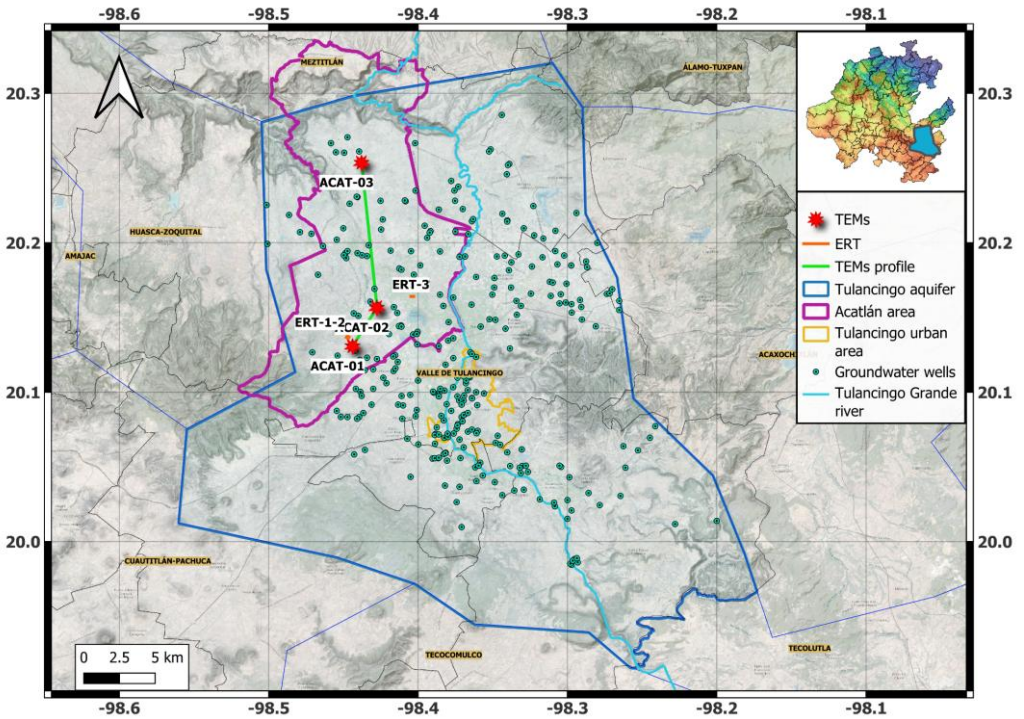


Fig. 1. Spatial location of the Tulancingo Valley aquifer. The aquifer is located in the southeast of the state of Hidalgo (blue polygon). Adjacent aquifers are labeled in yellow. The municipality of Acatlán is highlighted in magenta, while the metropolitan area of Tulancingo de Bravo is shown in yellow. Red stars indicate the location of the TEM surveys. ERT-1 and ERT-2 are located 750 m northwest of the TEM ACAT-01 survey, while ERT-3 is located ~2.5 km northeast of the TEM ACAT-02 survey. Green circles mark the groundwater wells in the region, according to the REPDA (2024, https://sigagis.conagua.gob.mx/locrepda20/). The Río Grande Tulancingo (cyan) follows a SE-NW trajectory that crosses the entire aquifer and continues northward.

Despite its regional importance and the rapid population growth in the metropolitan area of Tulancingo de Bravo, the subsurface geometry and hydraulic connectivity of the aquifer remain insufficiently understood. The most recent comprehensive geological-geophysical study was conducted nearly two decades ago (2). This lack of data compounds the challenge of sustainable management, primarily because the geological framework governing groundwater flow (such as the geometry of faults, fractures, and volcanic units) is poorly constrained.

In this context, geophysical methods offer a non-invasive and effective approach to characterizing these complex subsurface systems. Specifically, Electrical Resistivity Tomography (ERT) and Transient Electromagnetic (TEM) soundings have proven highly effective in identifying resistivity contrasts associated with lithological variations, groundwater saturation, and structural controls (e.g., 8, 9, 10, 11, 12, 13, 14, 15). While ERT

provides high-resolution 2D imaging of shallow structures and fracture networks, TEM soundings enhance deep conductive layers and regional stratigraphic sequences (e.g., 16, 17, 18, 19).

To address the knowledge gaps using an integrated approach, this study characterizes the hydrogeological structure of the northwestern Tulancingo Valley aquifer through an integrated analysis of structural trends by satellite gravimetric data and newly acquired TEM and ERT datasets. Specifically, this work aims to delineate the spatial extent and depth of both shallow and deep aquifer systems, identify structural controls of hydraulic connectivity and potential aquitard units, and establish a geophysical framework to support sustainable groundwater management in this highly stressed aquifer system.

2. Geological and hydrogeological setting

The Tulancingo Valley is located in the eastern part of the geological province known as the Trans-Mexican Volcanic Belt, bordering the Sierra Madre Oriental to the north (Fig. 2). It is characterized by a broad plain composed mainly of volcanic and sedimentary rocks, along with alluvial and fluvial sediments (20). The study area's basement consists of Mesozoic sedimentary rocks. The oldest unit is the Huizachal Formation, which includes siltstones, sandstones, and conglomerates, outcropping to the northeast. Overlying this are dark shales interbedded with sandstones, conglomerates, and limestones (Huayacocotla Formation), primarily outcropping to the northeast. Above these is the Soyatal Formation, a thick interbedded layer of shales and limestones, found mainly in the northern part of the study area within the Metztitlan ravine (Fig. 2).

The oldest Cenozoic volcanic rocks in the region correspond to the Pachuca Group, Navajas Rhyolite, and Atotonilco El Grande formations (Fig. 2). The Pachuca Group (Oligocene-Miocene) consists of lava flows, tuffs and breccias of rhyolitic composition, and dacitic lavas, mainly outcropping in the eastern part of the study area. The Navajas Rhyolite (Oligocene) consists of massive rhyolite flows, mainly outcropping in the western part. The Atotonilco el Grande Formation (Pliocene) includes pumice layers interbedded with pyroclastic and lithic material, as well as basalt flows, mainly found in the northern part. Other lithologies of lesser extent include the Calpulalpan Formation (tuffs, agglomerates, and volcanic gravel) and the Chignahuapan Rhyolite. During the Quaternary, basaltic, andesitic, and dacitic lava flows were deposited, interbedded with pyroclastic material, as well as the Guajolote Trachyte (Fig. 2). The most recent unit consists of alluvial and lacustrine sandy-clayey sediments (20).

The basement rocks in the Tulancingo Valley are folded due to the Mexican Orogen (21), though they only outcrop in the northern and northeastern parts of the study area. After compression ceased, normal and strike-slip faults were formed, creating tectonic basins. While regional faults do not outcrop in the valley, volcanic structures aligned within the area indicate faulting at depth (Fig. 2). Two main fault systems are identified, oriented NE-SW and NW-SE (2).

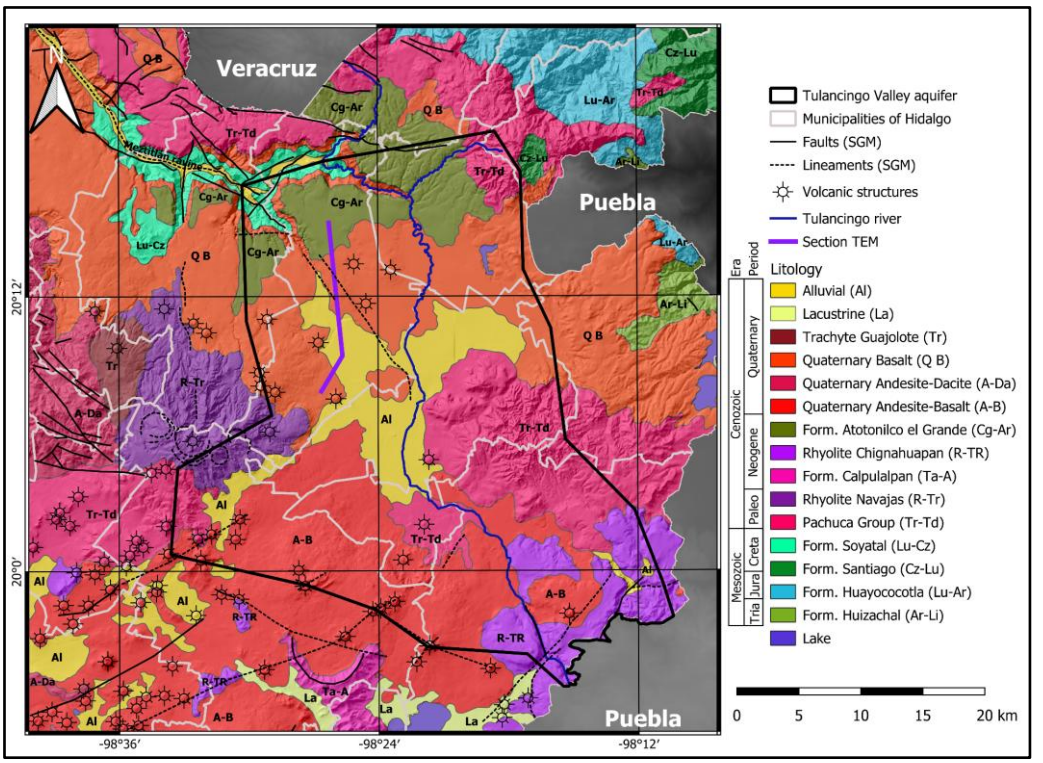


Fig. 2. Geology of the Tulancingo Valley region. The classification and color scale were derived from the Pachuca F14-11 mining geological map of the Mexican Geological Service (SGM). The faults and lineaments are reported by SGM.

The Tulancingo Valley aquifer is semi-confined and consists of three hydrogeological units. The first is a shallow granular unit (fluvio-alluvial sediments and pyroclastic materials), located in the southern part of the valley, with a thickness of 20 to 40 meters, and is exploited by wells and some shallow boreholes. The second, deeper unit extends across the valley and consists of pyroclastic deposits interbedded with tuffs, alluvial deposits, and basalt flows with thicknesses of up to 300 meters (2). Groundwater level in the northwest part of the aquifer varies between 50 m and 180 m (near the Meztitlan ravine), indicating

a northwestward flow (2). However, these depth levels were obtained in 2006 (Fig. 3). This flow is reflected in the Tulancingo Grande River, which originates in the northern mountains at SE, from the confluence of the San Lorenzo River, and runs through the Tulancingo Valley in a northwest direction, changing its name to Alcholoya River and later to Metztitlan River (5). This river is crucial for regional drainage and groundwater recharge. Also, it is worth noting that some lineaments are related to static level changes (Fig. 3).

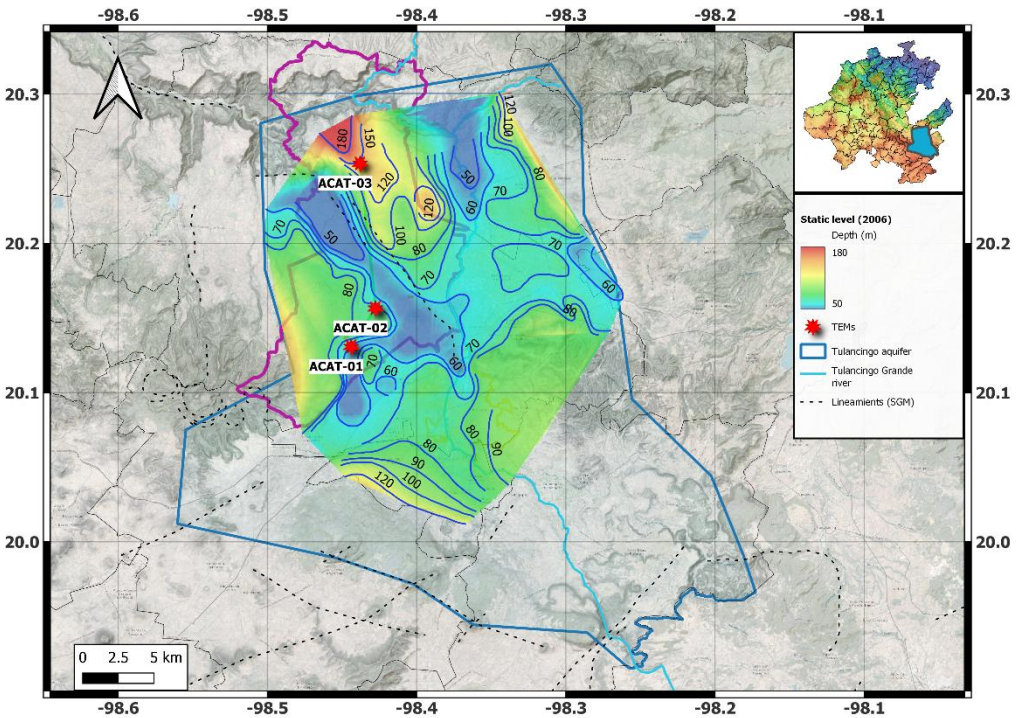


Fig. 3. Static groundwater level of the Tulancingo Valley aquifer estimated in 2006 (2).

3. Data and methods

3.1 Satellite gravity

The use of satellite gravimetric data facilitates the identification of regional lineaments that may correspond to geological structures such as faults and fractures that do not have surface expression in valleys such as the Tulancingo Valley. Satellite gravimetric data were obtained from the Global Gravity Model Plus (GGMPlus) project (22), which integrates GOCE/GRACE and EGM2008 satellite gravity surveys along with the implicit gravity effect in a terrain model filtered with a high-pass filter (see 22). The GGMPlus project provides free-air gravity anomalies, which were corrected for simple Bouguer, atmospheric, and terrain effects to yield the complete Bouguer anomaly. To determine the depths of regional and local sources, the radial power spectrum method was applied (23, 24). Shallow gravimetric lineaments were isolated by separating residual anomalies from the regional anomaly using a Butterworth filter. Finally, an analytical signal filter (e.g., 25) was applied to refine the localization of the lineaments.

3.2 Transient electromagnetic (TEM) survey

Three TEM surveys were conducted in the northwest of the Tulancingo aquifer, along the municipality of Acatlan (Fig. 1), using TerraTEM equipment designed by Monex GeoScope. The surveys utilized simple coils acting as both transmitters and receivers, arranged in square shapes with side lengths of approximately 275 m for the ACAT-01 survey and 200 m for the ACAT-02 and ACAT-03 surveys (Figs. 1 and 3). For data processing, a linear regression was applied to adjust the deeper signal, followed by an Occam inversion with a first-order smoothness regularization (26).

3.3 Electrical resistivity tomography (ERT)

For this study, the dipole-dipole configuration was used due to its sensitivity to horizontal resistivity changes (27). Field measurements were conducted using 48 electrodes spaced 1 m apart along a NW-SE-oriented line. The ERT-1 and ERT-2 geoelectrical sections were obtained to a depth of ~10 m to enhance the shallow details of the zone, while ERT-3 used the same 48 electrodes, but with 5 m spacing, reaching an investigation depth of ~60 m. The Ares I resistivimeter (GF Instruments) was used for data collection. During processing, spikes and anomalous values were removed, and inversion was performed using a first-order smoothness regularization.

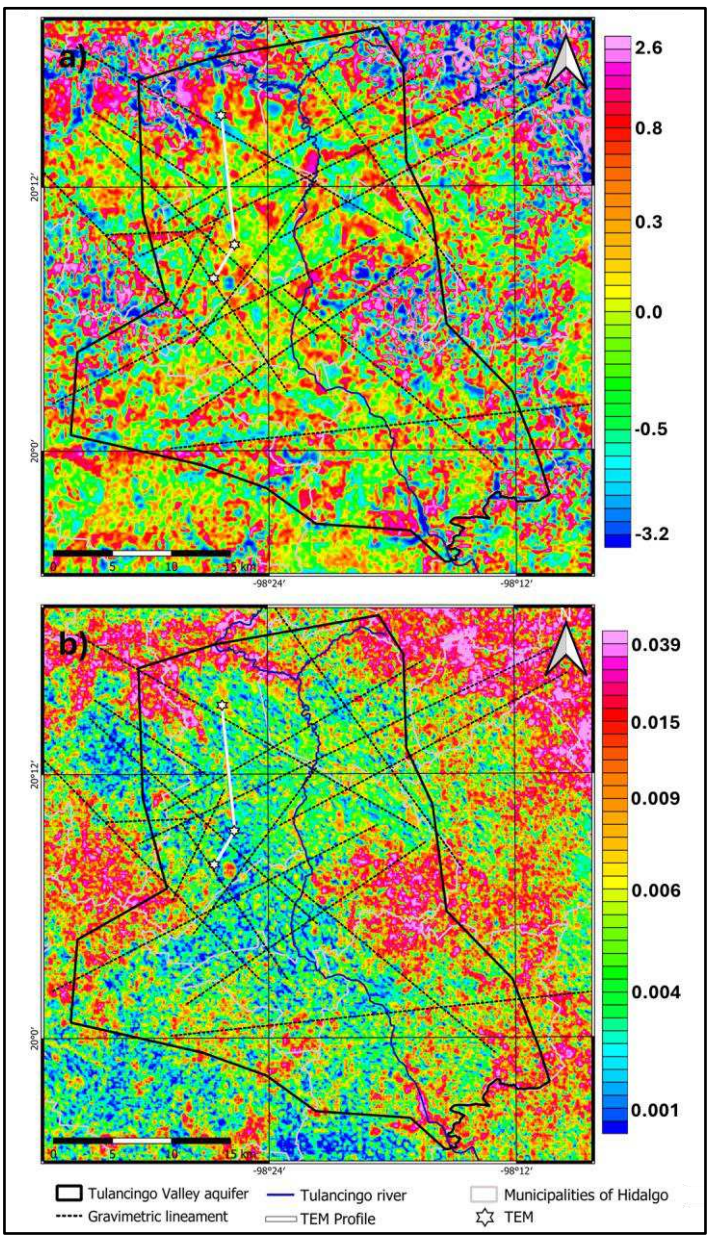
4. Results

The results are presented at both regional and local scales. Regional results focus on gravimetric lineaments used to identify buried structural features within the valley. Local results highlight resistivity contrasts that help to define the aquifer's dimensions. By integrating both sets of data, a general outline of the aquifer's geometry is derived, which is discussed in detail below.

4.1 Regional structural trends

The complete Bouguer anomaly ranges from -223.4 to -86.5 milligals. The depth of the regional sources was determined to be 5.6 km, while shallow sources were at 0.3 km. The residual gravimetric anomaly reveals several alignments (Fig. 4a), which are further highlighted by the analytical signal filter (Fig. 4b). Regional geophysical data indicate lineaments oriented NW-SE and NE-SW in the study area. Although no mapped regional faults are present, NW-SE-oriented faults and lineaments associated with the Acoculco

177 caldera have been documented in the southeastern part (28, 29). Additionally, normal
178 faults and NE-SW-oriented lineaments have been documented in the southern part of the
179 area (30, 31, 28, 32).



180

Fig. 4. a) Residual gravimetric anomaly; b) Analytical signal. Dashed lines represent gravimetric lineaments potentially correlated with geological faults.

4.2 TEM surveys

The TEM geoelectrical section is oriented SW-NE from station ACAT-01 to ACAT-02 and S-N from station ACAT-02 to ACAT-03, reaching a maximum depth of 360 m. Three geoelectric units are identified along the section (Fig. 5). Unit A (UA, blue tones) exhibits resistivities ranging from 1 to 20 Ω·m. It is observed in the SW and central portion of the profile. Below station ACAT-01, UA is located at a depth of 90-100 m, with an approximate thickness of 240 m. Below station ACAT-02, UA is at a depth of 160 m, with an approximate thickness of 160 m. Unit B (UB, green tones) exhibits resistivities from 21 to 50 Ω·m and is observed in the surface portion of the entire section. Beneath station ACAT-01, UB has a thickness of 10 m, while beneath station ACAT-02, it has a thickness of 160 m, and beneath station ACAT-03, it has a thickness of 280 m. Unit C (UC, yellow-red tones) has resistivities ranging from 51 to 120 Ω·m and is observed as a lens beneath all stations. At station ACAT-01, UC is located at a depth of 10 m with a thickness of 80 m; at station ACAT-02, it is at a depth of 70 m with a thickness of 60 m; and at station ACAT-03, it is located at a depth of 60 m with a thickness of 30 m. The gravimetric lineaments identified in this study are placed within the TEM section, indicating inferred regional geological faults (Fig. 5).

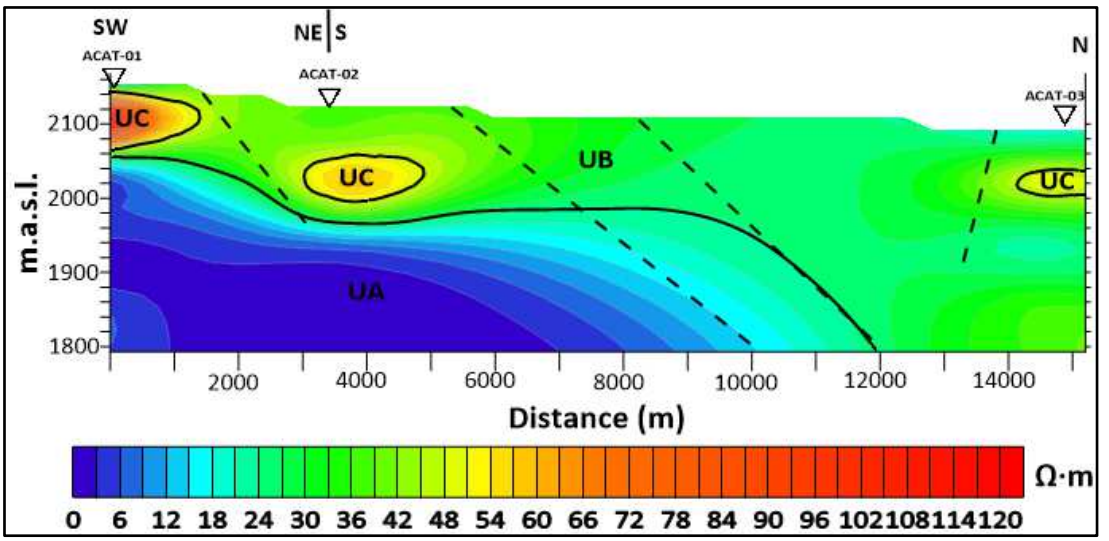


Fig. 5. Geoelectric section obtained from TEM surveys, showing three main units: UA (1-20 Ω·m), UB (21-50 Ω·m), and UC (51-120 Ω·m). m.a.s.l. refers to meters above sea level. Dashed lines represent lineaments correlated with geological faults.

4.3 Geoelectric resistivity tomographies

Geoelectric section TRE-1, oriented NW-SE and 47 meters long, reached a depth of 12 meters and reveals the contact between three geoelectric units (Fig. 6). Unit 1 (U1, dark blue tones), the shallowest, spans the SE portion of the section from 18 to 45 meters and has an average thickness of 7 meters. Its resistivity ranges from 1 to 30 Ω·m. Unit 2 (U2, light blue tones), located beneath U1, outcrops in the NW portion of the section from 5 to 15 meters, with an average thickness of 10 meters. The resistivities of U2 range from 31 to 140 Ω·m. Unit 3 (U3, green-orange tones), found in the NW portion of the section, extends from 0 to 5 meters, with a thickness of 5 meters. The resistivity of U3 varies from 141 to

360 Ω·m. In the central part, two discontinuities are observed between 19 and 25 meters, with a smaller discontinuity at 5 m (Fig. 6).

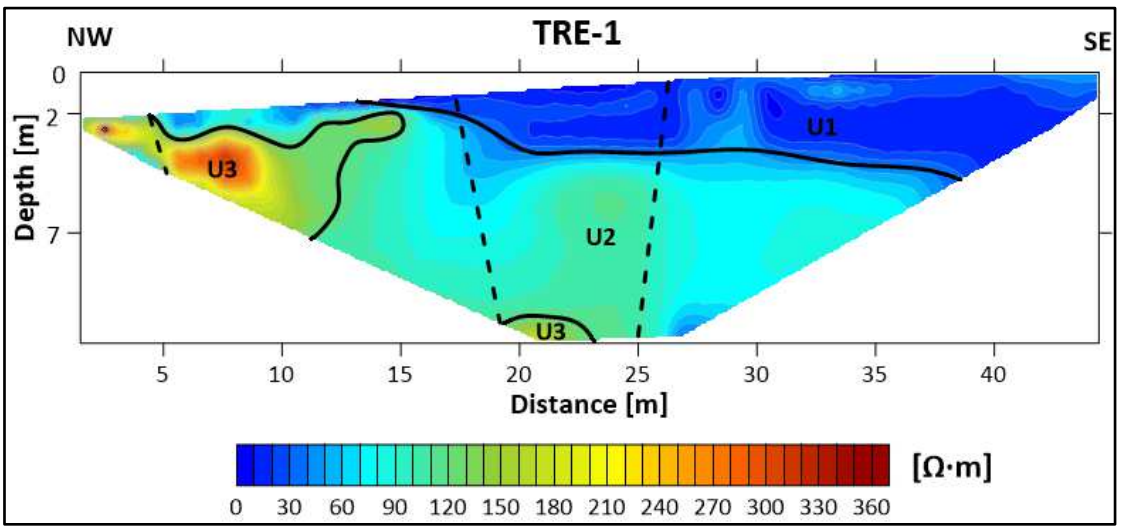


Fig. 6. Geoelectric section obtained from TRE-1 tomography. Three main units are observed: U1 (1-30 Ω·m), U2 (31-140 Ω·m), and U3 (141-360 Ω·m). The dashed lines represent lineaments that may correspond to geological faults or fractures. At 25 m, an artisanal well is located approximately 4 m from the section.

The TRE-2 section, oriented NW-SE and 45 meters long, reached a depth of 10 meters. This profile reveals the contact between three geoelectric units (Fig. 7). Unit 1 (U1, dark blue tones), the shallowest, has an average thickness of 4 meters, with resistivities ranging from 1 to 30 Ω·m. Unit 2 (U2, light blue-green tones) lies beneath Unit U1, with a thickness of 7 meters, and its resistivities range from 31 to 140 Ω·m. Unit 3 (U3, orange-red tones), located in the NW portion of the section between 8 and 12 meters, is at a depth of 2 meters, and has resistivities ranging from 141 to 180 Ω·m. Two discontinuities are observed in the

central part of the section at meters 17 and 23. The region between these discontinuities exhibits the lowest resistivity values of U2 (Fig. 7).

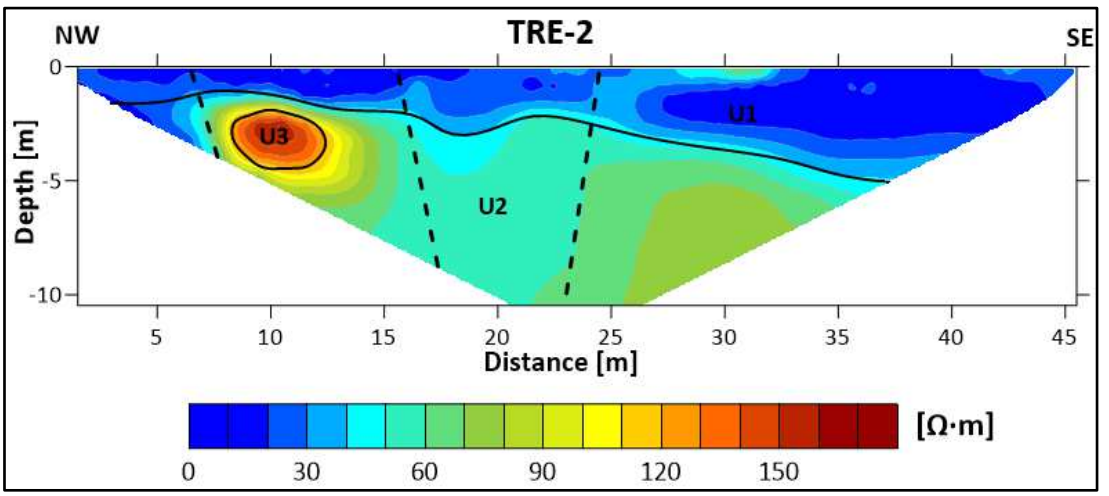


Fig. 7. Geoelectric section obtained from TRE-2 tomography. Three main units are observed: U1 (1-30 Ω·m), U2 (31-140 Ω·m), and U3 (141-180 Ω·m). The dashed lines represent lineaments that may correspond to geological faults or fractures.

The TRE-3 section, oriented nearly east-west and 182 meters long, reached a depth of 65 meters. This section reveals the contact between two geoelectric units (Fig. 8). The shallower unit (U1, blue tones) has an average thickness of 35 meters, with resistivities ranging from 1 to 30 Ω·m. Unit 2 (U2, yellow-red tones) beneath U1 within the section has a thickness of 35 m, with resistivities ranging from 31 to 80 Ω·m. A discontinuity is observed in the western part at meter 140.

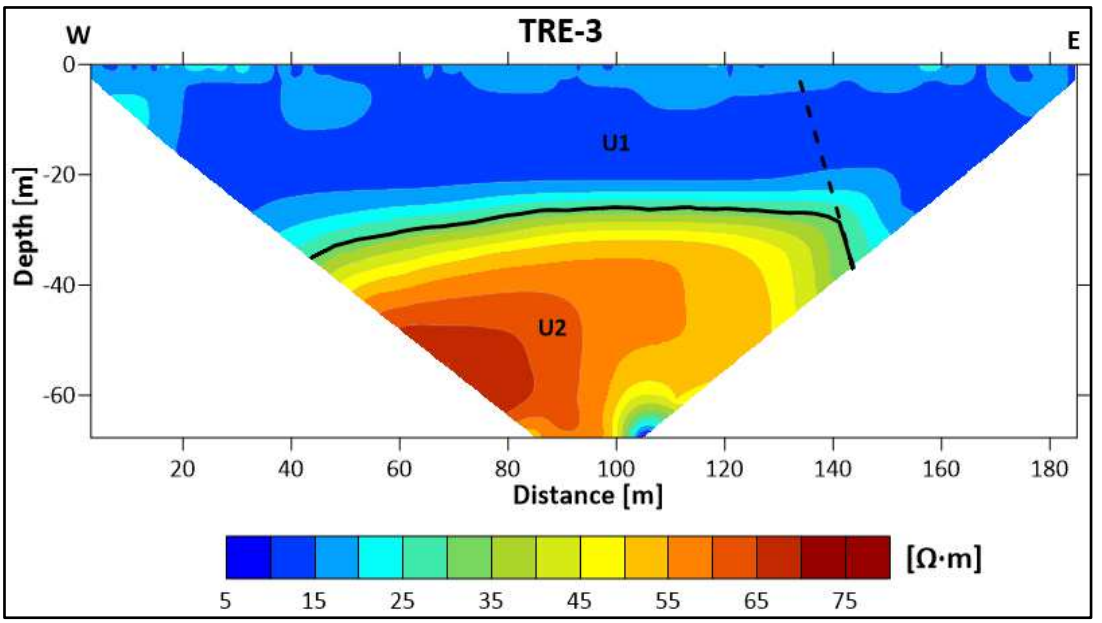


Fig. 8. Geoelectric section obtained from TRE-3 tomography. Two main units are observed: U1 (1-30 Ω·m) and U2 (31-80 Ω·m). The dashed line represents a lineament that may correspond with a geological fault.

5. Discussion

5.1 Geometry of the shallow aquifer

Using the TRE sections, three geoelectric units were delineated, reaching a maximum depth of 60 m (TRE-3, Fig. 8). These geoelectric units correlate with the following lithologies: Unit U1 corresponds to the alluvial fill covering the central part of the Tulancingo Valley. Within the TRE-1 and TRE-2 sections, it reaches a maximum thickness of 5 m, while in the TRE-3 section, it has a general thickness of 35 m. Unit U2 corresponds to highly fractured basalt, predominantly outcropping in the NW portion of the TRE-1 and TRE-2 sections, with a

thickness of 8 m; in TRE-3, it exceeds 25 m. Unit U3 corresponds to fresher basalt, located only in the NW portion of TRE-1 and TRE-2.

According to the Mexican Geological Survey (20), profiles TRE-1 and TRE-2 are located in Quaternary fissure basalts (Fig. 9a). These basalts exhibit a blocky lava structure (50 cm to 1 m), indicating a highly fractured basalt with vesicles (Fig. 9b), which results in lower resistivity values than expected for a fresh basalt (Fig. 10). Conversely, the relatively high resistivity values of unit U3 observed at the NW portion of the profiles may correspond to fresh basalt without vesicles and with fewer fractures near the source, perhaps related to local fractures or faults. In TRE-3, only units U1 and U2 are observed, corresponding to alluvial fill and fractured basalts (Fig. 10).

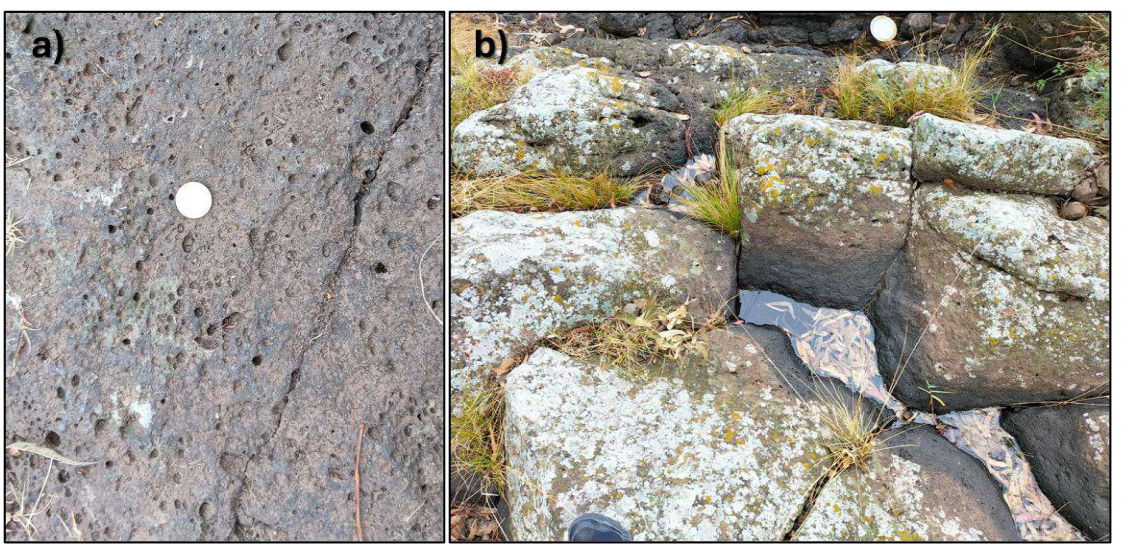
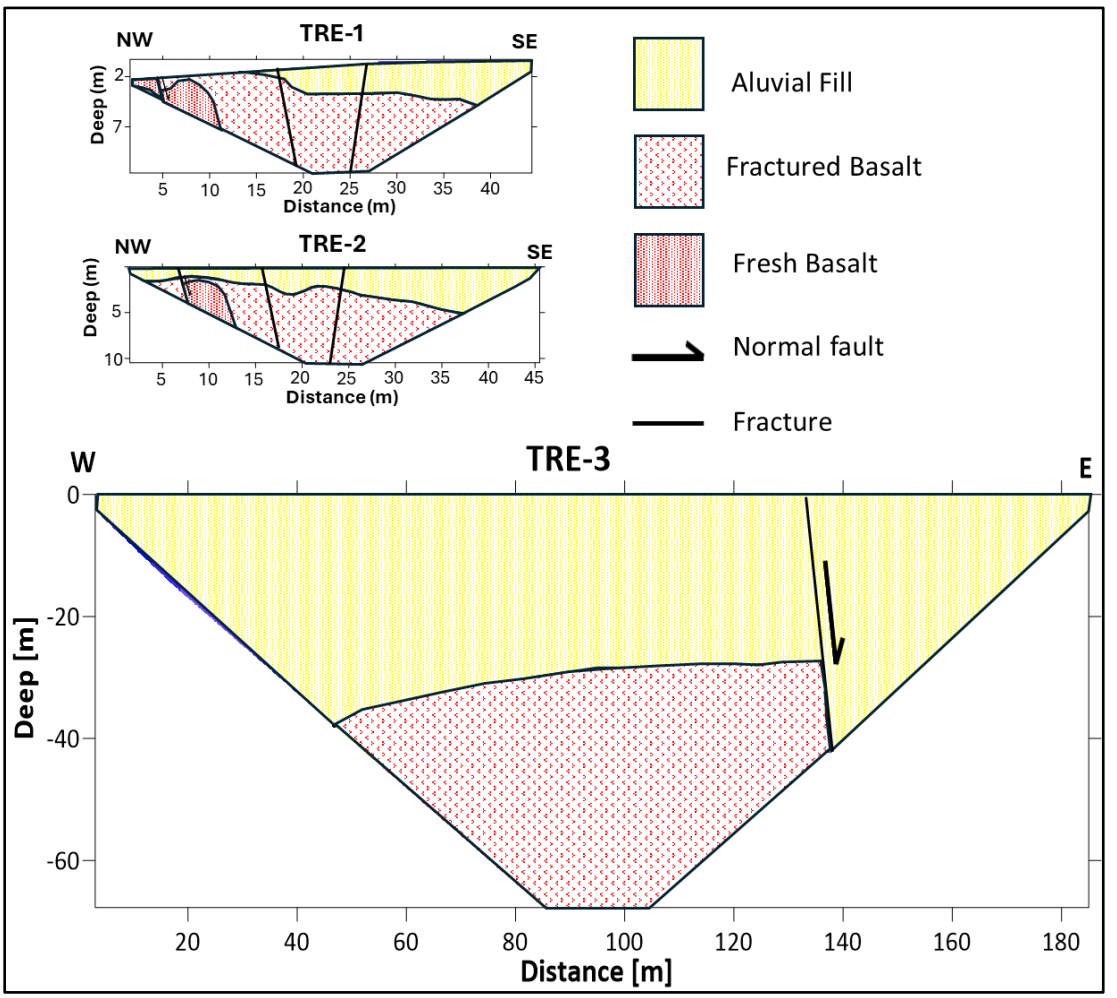


Fig. 9. Quaternary fissure basalts in Acatlán. (a) Vesicular Quaternary Basalt. (b) Quaternary fissural basalt in blocks cut by fractures.

In the TRE-1 and TRE-2 sections, three nearly vertical discontinuities are observed, which may be faults or fractures separating the basalt into blocks. These discontinuities also act as boundaries between zones of greater and lesser deformation. The zones of greater deformation exhibit a higher fracturing density and are distinguished in the profiles by lower resistivities (light blue tone). In the NW part of both sections, the basalts that outcrop in the stream have two main fracture sets, one with a NW-SE orientation (327° average strike), and the other with a NE-SW orientation (038° average strike). Therefore, the faults and fractures observed in the resistivity sections could correspond to those with a general NE-SW orientation. The TRE-3 section, on the other hand, shows a discontinuity in its eastern part. This discontinuity is interpreted as a normal fault with its hanging wall block on the right (Fig. 10).

Based on data obtained from electrical resistivity tomography (Fig. 8), the presence of a shallow aquifer can be inferred to be hosted within alluvial deposits and fractured vesicular basalts. Meanwhile, the fresher basalts may act as barriers restricting groundwater flow, and geological faults may act as conduits connecting the shallow aquifer to the deep aquifer. Towards the southeastern (SE) part of the ERT-1 and ERT-2 sections, there is an artificial excavation related to artisanal groundwater exploitation wells (Fig. 6), where water is extracted at a depth of ~5 m. This artificial deposit spatially coincides with the low resistivity anomalies observed in Figs. 6 and 7, and the fresher basalts could act as barriers restricting vertical flow. However, the spatial distribution of these fresh basalts throughout the aquifer is unknown. Tomographic surveys suggest they are found at the surface in the

284 westernmost part of the aquifer (TRE-1 and TRE-2), while they are found at greater depths
285 towards the central area (TRE-3). Therefore, the shallow aquifer in the westernmost part
286 of the aquifer may be a local perched aquifer, trapped between basalt flows.



287

288 Fig. 10. Interpreted geoelectrical ERT sections.

289 **5.2 Groundwater flow through the deep aquifer**

Using the TEM section, three geoelectric units were delineated, reaching a maximum depth of 300 meters (Fig. 5). Unlike the TRE profiles, a single lithology cannot be assigned to each geoelectric unit. Generally, the Unit UA corresponds to the lithology of the Pachuca Group (Fig. 11). The Unit UB exhibits the lithology of the Atotonilco El Grande Formation, Quaternary basalts, basalt flows, and alluvial fill (Fig. 11). In the SW part of the section under the ACAT-01 station, the basalt flows correspond to the fractured vesicular basalts seen in the TRE sections (Figs. 6, 7, and 8). The Unit UC corresponds primarily to Quaternary basalts with few fractures in the SW portion of the section and to the Atotonilco El Grande Formation with few fractures in the N portion of the section (Fig. 11).

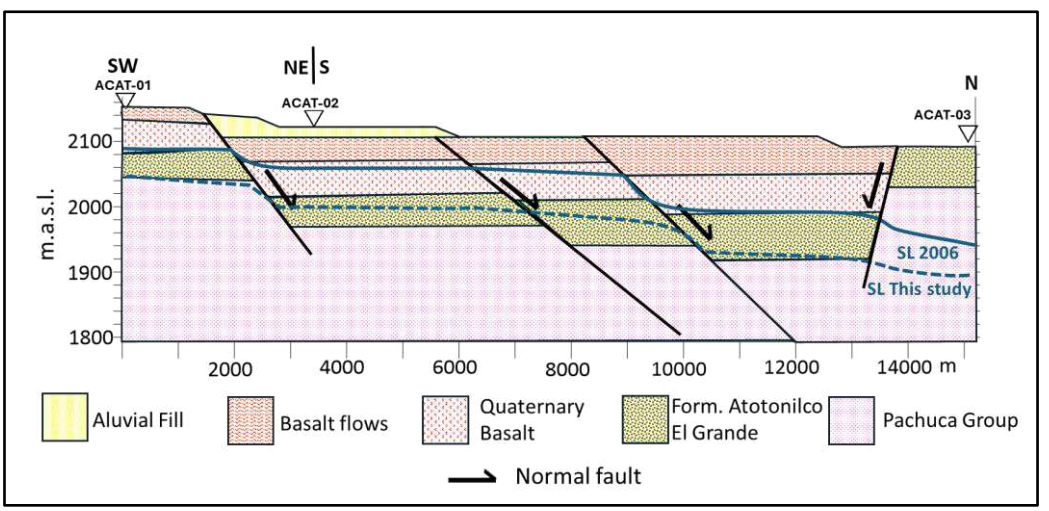


Fig. 11. Schematic geological section of the TEM profile. The solid blue line corresponds to the static water level established by CONAGUA (2). The dashed blue line corresponds to the static water level estimated in this study. SL: static water level.

According to CONAGUA (2), the deep aquifer is located at a depth of 60-150 m (Fig. 3). Between stations ACAT-01 and ACAT-02, the static water level is at an approximate depth of 70 m. Between stations ACAT-02 and ACAT-03, from south to north, the water level is 70 m, rises to 60 m, and then drops to 150 m. Fig. 11 shows the static water level estimated by CONAGUA (2), as well as the estimate in this study based on the resistivity values obtained from the TEM soundings. In this study, the inferred static level coincides with the upper limit of the UA unit for the central and SW portion of the TEM profile (Fig. 5). Towards the N portion of the profile, the static level coincides with a geoelectric change from 18 to 30 Ω·m (light blue to green tones). To verify the decrease in the static level, it is necessary to conduct piezometric measurements in the deep-water wells.

A very abrupt drop (approximately 40 m) in the static water level at 10 km along the section can be observed; this drop coincides with the trace of a fault inferred in this study. The drop in the static water level to 150 m in the northern part of the profile coincides with the lithological change in the Pachuca Group. Within the Metztitlán ravine, andesitic lavas are observed that correlate with the Pachuca Group, which are overlain by the Atotonilco el Grande Formation, and at the top of the ravine are located Quaternary basalts (Fig. 12).

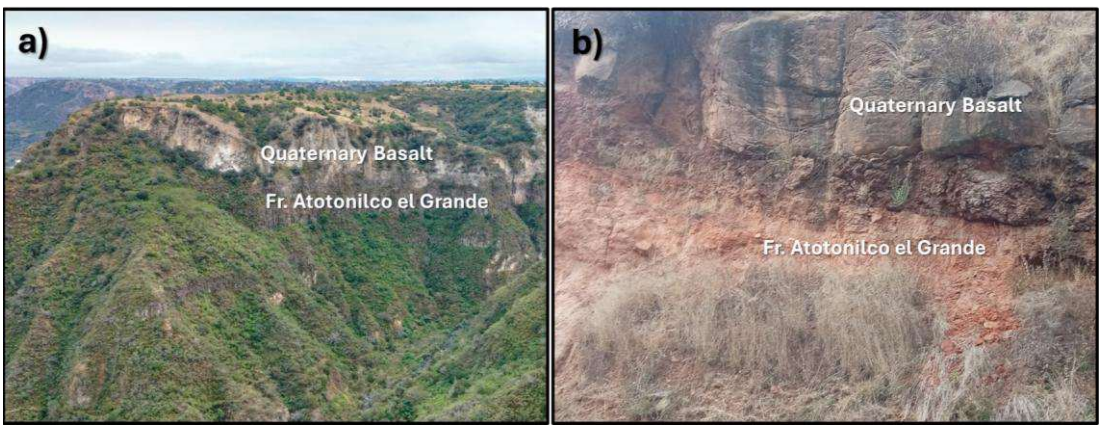


Fig. 12. Exposed geological contact in the northwest of the aquifer. (a) Contact between the Atotonilco el Grande Formation and the Quaternary Basalts at the top of the Meztitlán canyon. (b) Contact between the Atotonilco el Grande Formation and the Quaternary Basalts on the Acatlan-Huasca highway.

On the other hand, due to the lack of data between stations ACAT-02 and ACAT-03 in the TEM section, discontinuities and artifacts could be generated by the interpolation, which do not reflect the true geometry of the geohydrological units. However, the existence of regional faults in the southern part of the aquifer with NE-SW and NW-SE orientations (30, 31, 28, 29, 32), the gravimetric lineaments identified in this study, the NE-SW oriented lineaments identified by the SGM (Fig. 2), and the surface distribution of the lithology mapped by the SGM (Quaternary basalts and alluvial fill; Ramírez-Tello et al. (30)), support the possible connection between the structures proposed in the TEM section and the presence of buried regional faults in the Valley.

5.3 Interaction between a shallow and a deep aquifer

Based on the TRE data, a shallow aquifer is assumed to be present, hosted in alluvial deposits and basalt flows, with an approximate thickness of 30 m in the central part of the valley (Fig. 10). TEM surveys suggest the presence of an aquitard separating the shallow aquifer from the deep aquifer. Below the aquitard lies the deep aquifer, hosted in the Atotonilco El Grande Formation and the Pachuca Group (Fig. 11). The thickness of the deep aquifer cannot be determined using the TEM section, but it is assumed that the basement of the entire basin consists of Cretaceous carbonate rocks (2). According to Ramírez-Tello et al. (33) and CONAGUA (2), the basement is located at a depth of 400 to 500 m. In this way, the thickness of the deep aquifer could vary between 300 and 400 m.

The presence of an aquitard between the shallow and deep aquifers limits communication between them solely to geological faults. This aquitard corresponds to Quaternary basalts observed at the top of the Meztitlan ravine, where they appear as massive basalts (Fig. 12). According to the gravimetric data processed in this study and by various authors (30, 31, 28, 20, 29, 2), there are at least two regional fault systems that cross the Tulancingo Valley or are on the periphery of the valley (NE-SW and NW-SE orientations) and may cut across this aquitard. Thus, the two aquifers are connected through these faults.

Geological faults can control groundwater flow. They act as conduits that maximize water flow or, conversely, as barriers that slow and redistribute it (36, 35, 8, 36, 37, 38, 39). Within the study area, abrupt changes in the static water level are observed, which can be associated with the presence of faults. Fig. 11 shows that the faults located at 2.5 km and 10 km coincide with these abrupt changes in the static water level. Therefore, it is

355 important to consider that the presence of faults, their size, and their orientation play a
356 significant role in controlling groundwater flow in the Tulancingo Valley aquifer, and these
357 structures should be taken into account in decision-making regarding aquifer water
358 management.

359 **5.4 Implications for groundwater management**

360 Groundwater availability in the Tulancingo Valley aquifer exhibits a clear and persistent
361 deficit trend over time (Fig. 13). This decline is exacerbated by intense anthropogenic
362 pressure, as the population of Tulancingo de Bravo grew from 126,000 in 2006 to 168,369
363 in 2020. Such conditions present significant socio-environmental challenges, highlighting
364 an urgent need for comprehensive and periodic monitoring of the aquifer's hydrogeological
365 behavior. Furthermore, TEM data indicate an estimated 40-meter drop in the static water
366 level over the last 20 years (Fig. 11). If this trend continues, projected water deficits for
367 2030 and 2050 could reach 23.64 Mm^3 and 31.64 Mm^3, accompanied by additional drops
368 in static levels of 20 and 50 m, respectively. This scenario would require deeper wells,
369 leading to higher extraction costs and increased vulnerability of the region’s groundwater
370 resources.

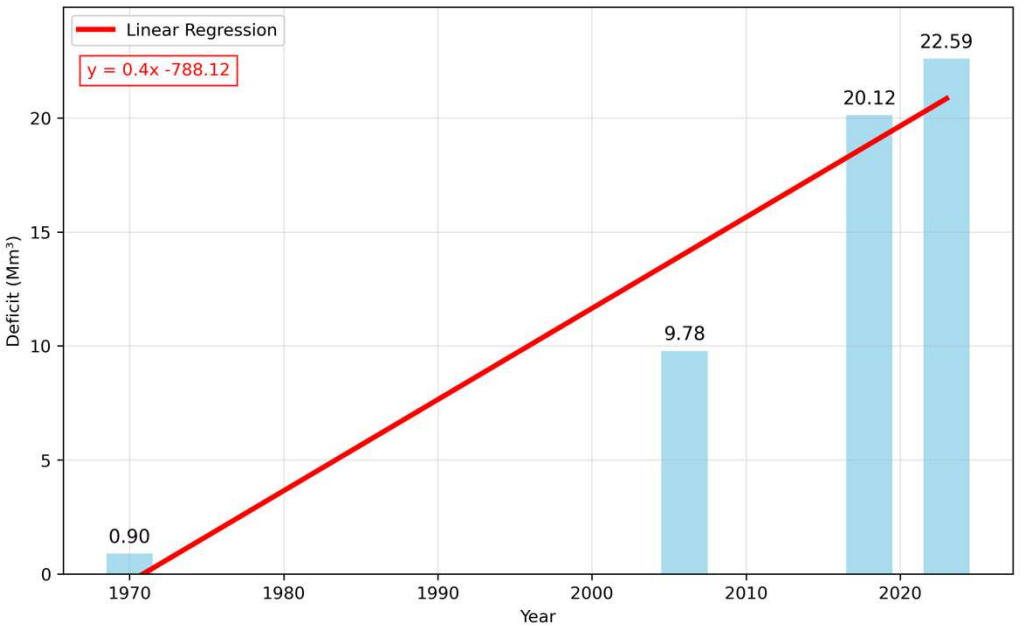


Fig. 13. Temporal variation in the aquifer's volume deficit (2, 40). For the 1966-1973 period, the average was used (CONAGUA, 2006). The red line shows the linear trend of the deficit.

6. Conclusions

Our analyses of integrated gravity and geoelectrical studies in the northwestern Tulancingo Valley aquifer revealed the following significant findings:

1.- The integrated geoelectrical and TEM study shows that the Tulancingo Valley aquifer is a complex, multi-layered system, comprising a shallow aquifer hosted in alluvial deposits and fractured basalts, an intermediate volcanic aquitard, and a deep aquifer hosted in the Atotonilco El Grande Formation and the Pachuca Group. The shallow aquifer reaches up to 35 m in thickness, while the deep aquifer may extend 300–400 m.

2.- Gravimetric and geoelectrical data indicate the presence of regional and shallow structural lineaments that influence groundwater flow. These lineaments, oriented NW-SE and NE-SW, act as conduits or barriers, controlling connectivity between aquifer units.

3.- Geological structures, particularly faults and fractures, critically control groundwater flow. Faults act both as conduits connecting the shallow and deep aquifers and as barriers that redistribute flow, producing abrupt changes in static water levels. Two major regional fault systems (NE-SW and NW-SE) intersect the valley, strongly influencing aquifer connectivity and hydraulic behavior.

4.- By varying the resistivity values obtained from the TEM and TRE, a decrease in the groundwater level is estimated over the last two decades, with an estimated 40-meter drop in static water levels. Population growth and intense anthropogenic extraction exacerbate this trend, resulting in a persistent deficit in water availability.

5.- Projections suggest that if current extraction trends continue, water deficits could reach 23.64 Mm^3 by 2030 and 31.64 Mm^3 by 2050, accompanied by further declines in static water levels of up to 50 m. This scenario would require deeper wells, increasing extraction costs and amplifying the vulnerability of groundwater resources.

These findings highlight the urgent need for strategic and sustainable groundwater management, including periodic monitoring, regulation of extraction, and consideration of structural controls in planning. The geophysical framework established in this study, combining gravimetric and geoelectrical data, provides a robust scientific basis for

transitioning from reactive exploitation to proactive, long-term management of the most overexploited aquifer in Hidalgo.

Acknowledgments

We thank Jorge López Alviz for his suggestions and comments to enhance the quality of the paper. To the technical engineers Rubén Darío Valle Orozco, César Raymundo Tapia Aguilar, Alejandro Zárate Requena, Jesús Guizar Jardón, Ricardo Omar Venegas Sánchez, Omar Rosas, Jesrel Álvarez Becerra, Gabriel Castillo Aparicio and Juan Ramón Albañez Domínguez for their valuable help with the instrument's operation and the acquisition of field data. This project was supported by the PhD SECIHTI scholarship no. 538423 and the 153/2025 grant from the DGAPA POSDOC program at UNAM.

Ethics statement

Ethics, Consent to Participate, and Consent to Publish declarations: not applicable.

Availability of Data and Materials

Data are available upon request directly from the corresponding author.

Funding Information and Conflicts of Interest

The authors declare that they have no known competing financial interests or personal relationships that could have appeared to influence the work reported in this paper.

Author Contributions

DAAA: Conceptualization, methodology, formal analysis, investigation, project administration, funding, data curation, writing original draft, review & editing. ***GCV:*** Conceptualization, methodology, data acquisition, writing original draft, review & editing. ***FCH:*** Validation, writing original draft, review & editing. ***AISA:*** Data curation, review & editing.

References

1 Del Villar K.E. (2014). Agua, Estudio Hidrológico: Problemática y soluciones en la Cuenca de la región de Tulancingo (Tomo 1). Confederación de Organismos Agropecuarios del Estado de Hidalgo-Universidad Politécnica de Tulancingo, p. 17-25

2 CONAGUA. (2024). Actualización de la disponibilidad media anual de agua en el acuífero Valle de Tulancingo (1317). Estado de Hidalgo.

3 Gómez Alcántara, A., Cervantes Escoto, F., Altamirano Cárdenas, J. R., & Garza López, J. Ma. (2009). Alternativas a la problemática ocasionada por lactosueros en el Valle de Tulancingo, Hidalgo.

4 Guerrero Rodríguez, W. J., Gómez Aldapa, C. A., Castro Rosa, J., González Ramírez, C. A., & Santos López, E. M. (2010). Caracterización fisicoquímica del lactosuero en el Valle de Tulancingo. XII Congreso nacional de ciencia y tecnología de alimentos. Guanajuato, México.

5 Sánchez Misael, C., Anallely, A. O., Monzalvo Vanessa, M., García Patricia, G., Luna, S., & Cecilia, M. (2020). Hidroquímica e índice de calidad del Acuífero del Valle de Tulancingo, Hidalgo, México. Universidad Autónoma Metropolitana Revista Tediq, 6(6), 147–156.

6 Cruz-Sánchez, M., Lobaco-Mejía, V., Esquivel-Macías, C., Ramírez-Cardona, M., & Flores-Castro, K. (2022). Evaluación del Acuífero Valle de Tulancingo para propósitos de irrigación. Tópicos de Investigación en Ciencias de la Tierra y Materiales, 9(9), 39–46. https://doi.org/10.29057/aactm.v9i9.9513

7 Espinoza Juárez, T. K., Morales-Arredondo, J. I., Armienta Hernández, M. A., Caccavari Garza, A. L., Cifuentes Nava, G., Pérez-Calderón, D. A., Mosso-Mendoza, E. A. (2026). Application of geophysical and hydrogeochemical methods in the Zimapán Aquifer, Hidalgo for environmental purposes. Geofísica Internacional, 65(2), 2071–2088. https://doi.org/10.22201/igeof.2954436xe.2026.65.2.1916

8 Berkowitz, B. (2002). Characterizing flow and transport in fractured geological media: A review: Advances in Water Resources 25, 861–884. https://doi.org/10.1016/s0309-1708(02)00042-8

9 Arango-Galván, C., de la Torre-González, B., Chávez-Segura, R.E., Tejero-Andrade, A., Cifuentes-Nava, G. and Hernández-Quintero, E. (2011). Subsidence structural pattern defined in a habitational complex of the southeastern zone of the Mexico Basin inferred from electrical resistivity image: Geofísica Internacional, 50, 401–409.

10 Chavéz, R., Tejero, A., Cifuentes-Nava, G., Hernández-Quintero, J. E. & Aguilar, D. A. (2015). Imaging Fractures beneath a Residential Complex Using Novel 3-D Electrical Resistivity Arrays. Journal of Environmental & Engineering Geophysics. 20. 219-233. 10.2113/JEEG20.3.219.

11 Batista-Rodríguez, J. A., Pérez-Flores, M. A., Almaguer-Carmenates, Y., Blanco-Moreno, J. A., López-Saucedo, F. de J., & Batista-Cruz, R. Y. (2021). Using electrical resistivity tomography to evaluate the relationship between groundwater potencial and tectonism in northeast Mexico. *Revista Mexicana De Ciencias Geológicas*, *38*(1), 18–28. https://doi.org/10.22201/cgeo.20072902e.2021.1.1597

12 Christensen, N.B., Sørensen, K.I. (1998). Surface and borehole electric and electromagnetic methods for hydrogeological investigations. European Journal of Environmental and Engineering Geophysics 3, 75–90.

13 Massoud, U., Qady, G. E., Metwaly, M., Santos, F. (2009). Delineation of shallow subsurface structure by azimuthal resistivity sounding and joint inversion of VES-TEM data: Case study near Lake Qaroun, El Fayoum, Egypt. Pure and Applied Geophysics, 166, 701-719.

14 Korus, J. T., R. M. Joeckel, D. Divine. (2013). Three-dimensional hydrostratigraphy of the Firth, Nebraska area: results from helicopter electromagnetic (HEM) mapping in the Eastern Nebraska Water Resources Assessment (ENWRA).

15 Auken, E., Foged, N., Larsen, J.J., Lassen, K.V.T., Maurya, P.K., Dath, S.M., Eiskjær, T.T. (2019). tTEM-A towed transient electromagnetic system for detailed 3D imaging of the top 70 m of the subsurface," Geophysics, vol. 84, no. 1, pp. E13-E22.

16 McNeill, J.D. (1994). Principles and Application of Time Domain Electromagnetic Techniques for Resistivity Sounding. Technical Note TN-27, Geonics Ltd., Ontario.

17 Ruiz-Aguilar, D., Tezkan, B., & Arango-Galván, C. (2018). Exploration of the Aquifer of San Felipe Geothermal Area (Mexico) by Spatially Constrained Inversion of Transient Electromagnetic Data. *Journal of Environmental and Engineering Geophysics*, *23*(2), 197–209. https://doi.org/10.2113/jeeg23.2.197

18 Torres-Martinez, J.A., Mora, A., Ramos-Leal, J.A., Janete Morán-Ramírez, Arango-Galván, C., Jürgen, M. (2019). Constraining a density-dependent flow model with the transient electromagnetic method in a coastal aquifer in Mexico to assess seawater intrusion. Hydrogeol J 27, 2955–2972. https://doi.org/10.1007/s10040-019-02024-w

19 Xian, J., He, Z., Hu, X., Liu, L., Auken, E., Revil, A., Cai, H. (2024). Groundwater Mapping and Modeling Using Towed Transient Electromagnetic Data Based on Deep Learning. IEEE Transactions on Geoscience and Remote Sensing.

20 SGM (2009). Servicio Geológico Mexicano, Ordenamiento Ecológico Territorial de la Región de Tulancingo. http://docencia.uaeh.edu.mx/estudios-pertinencia/docs/hidalgo-municipios/Tulancingo-Ordenamiento-Ecologico-Territorial.pdf

21 Fitz-Díaz, E., Lawton, T. F., Juárez-Arriaga, E., & Chávez-Cabello, G. (2018). The Cretaceous-Paleogene Mexican orogen: Structure, basin development, magmatism and tectonics. *Earth-Science Reviews*, *183*, 56-84.

22 Hirt, C., Claessens, S., Fecher, T., Kuhn, M., Pail, R., Rexer, M. (2013). New ultrahigh-resolution picture of Earth's gravity field, Geophysical Research Letters, 40, 4279-4283. https://doi.org/10.1002/grl.50838

23 Spector, A., Grant, F.S. (1970). Statistical models for interpreting aeromagnetic data. Geophysics 35, 293-302. https://doi.org/10.1190/1.1440092

24 Chávez, R.E., Lazaro-Mancilla, O., Campos-Enríquez, J.O., Flores-Márquez, E.L. (1999). Basement topography of the Mexicali Valley from spectral and ideal body analysis of gravity data, Journal of South American Earth Sciences, 12, 579-587. https://doi.org/10.1016/S0895-9811(99)00041-3

25 Nabighian, M.N. (1972). The analytic signal of two-dimensional magnetic bodies with polygonal cross-section; its properties and use for automated anomaly interpretation, Geophysics, 37, 507–517. https://doi.org/10.1190/1.1440276

26 Constable, S. C., Parker, R. L., & Constable, C. G. (1987). Occam's inversion: A practical algorithm for generating smooth models from electromagnetic sounding data. In GEOPHYSICS (Vol. 52, Number 3).

27 Loke, M. H. (2004). Tutorial: 2-D and 3D electrical imaging surveys.

514 28 López-Hernández, A. (2009). Evolución volcánica del Complejo Tulancingo-Acocolco y
515 su sistema hidrotermal, Estados de Hidalgo y Puebla, México. PhD Thesis, Universidad
516 Nacional Autónoma de México.

517 29 Solana-López, J. (2010). Geología regional y petrogénesis del vulcanismo silícico de la
518 región circundante a la ciudad de Tulancingo, Estado de Hidalgo, Master Thesis, Instituto
519 Politécnico Nacional.

520 30 García-Palomo, A., Macías, J.L., Tolsón, G., Valdez, G., Mora, J.C. (2002). Volcanic
521 stratigraphy and geological evolution of the Apan region, east-central sector of the Trans-
522 Mexican Volcanic Belt, Geofísica Internacional, 41, 133-150.
523 https://doi.org/10.22201/igeof.00167169p.2002.41.2.282

524 31 Campos-Enríquez, J.O., Alatriste-Vilchis, D.R., Huizar-Álvarez, R., Marines-Campos, R.,
525 Alatorre-Zamara, M.A. (2003). Subsurface structure of the Tecocomulco sub-basin
526 (northeastern Mexico basin), and its relationship to regional tectonics, Geofísica
527 Internacional 42, 3-24. https://doi.org/10.22201/igeof.00167169p.2003.42.1.356

528 32 García-Tovar, G.P., Martínez-Serrano, R.G., Solé, J., Correa-Tello, J.C., Núñez-Castillo, E.Y.,
529 Guillou, H., Monroy-Rodríguez, E. (2015). Geología, geocronología y geoquímica del
530 vulcanismo Plio-Cuaternario del Campo Volcánico Apan-Tecocomulco, Faja Volcánica
531 Trans-Mexicana, Revista Mexicana de Ciencias Geológicas, 32, 100-122.

532 33 Ramírez-Tello, E., Uribe-Luna, J., Galeana-Galicia, O.A., Torres-Ramírez, M., Bahena-
533 Estrada, F.M., Luna-Castro, H.F. (2016). Carta geológica Minera Tulancingo F14-D82,
534 1:50,000, Servicio Geológico Mexicano, primera edición.

535 34 Caine, J.S., Evans, J.P., Forster, C.B. (1996). Fault zone architecture and permeability
536 structure: Geology 24, 1025. https://doi.org/10.1130/0091-
537 7613(1996)024<1025:fzaaps>2.3.co;2

538 35 Rawling, G.C., Goodwin, L.B., Wilson, J.L. (2001). Internal architecture, permeability
539 structure, and hydrologic significance of contrasting fault-zone types: Geology, 29, 43–46.
540 https://doi.org/10.1130/0091-7613(2001)029<0043:IAPSAH>2.0.CO;2

541 36 Bense, V.F., Gleeson, T., Loveless, S.E., Bour, O., Scibek, J. (2013). Fault zone
542 hydrogeology: Earth-Science Reviews, 127, 171–192.
543 https://doi.org/10.1016/j.earscirev.2013.09.008

544 37 Moya, C.E., Raiber, M., Cox, M.E. (2014). Three-dimensional geological modelling of the
545 Galilee and central Eromanga basins, Australia: New insights into aquifer/aquitard
546 geometry and potential influence of faults on inter-connectivity: Journal of Hydrology:
547 Regional Studies, 2, 119–139. https://doi.org/10.1016/j.ejrh.2014.08.007

548 38 Ochoa-González, G. M., Carreón-Freyre, D., Cerca, M. and López-Martínez, M. (2015).
549 Assessment of groundwater flow in volcanic faulted areas. A study case in Queretaro,
550 Mexico: Geofísica Internacional. 54:199-220. https://doi.org/10.1016/j.gi.2015.04.016

551 39 Barrera-de-Calderón, M., Garfias, J., Martel, R., Salas-García, J. (2021). Controles
552 geológicos en el flujo de agua subterránea y distribución de volúmenes de extracción
553 asociados a una estructura volcánica compleja: Boletín de la Sociedad Geológica Mexicana,
554 73 (1), A170820 10.18268/BSGM2021v73n1a170820.

555 40 CONAGUA. (2018). Actualización de la disponibilidad media anual de agua en el acuífero
556 Valle de Tulancingo (1317). Estado de Hidalgo.